En Route to Ultrahigh Field Cardiac MR in Patients: RF Safety Assessment of Intracoronary Stents at 7.0 T Using Numerical Simulations and E-Field Measurements

Eva Oberacker[1], Lukas Winter[1], Frank Seifert[2], Jaroslav Marek[1], Gerd Weidemann[2], Eugen Hofmann[3], and Thoralf Niendorf[1,4]

[1]*Berlin Ultrahigh Field Facility (B.U.F.F.), Max Delbrück Center for Molecular Medicine, Berlin, Berlin, Germany,* [2]*Physikalisch Technische Bundesanstalt, Berlin, Germany,* [3]*Biotronik AG, Bülach, Switzerland,* [4]*Experimental and Clinical Research Center, a cooperation of the Charité Medical Faculty and the Max Delbrück Center for Molecular Medicine, Berlin, Germany*

Target audience: Basic researchers and clinical scientists interested in MR safety considerations for scanning subjects with intracoronary stents at ultrahigh fields

Purpose: A growing number of reports eloquently speak about explorations into cardiac magnetic resonance (CMR) at ultrahigh magnetic fields (UHF, $B_0 \geq 7.0$ T) [1]. Practical concerns are driving the notion that intracoronary stents are considered to be contraindications *per se* for UHF-CMR. Arguably, this notion is somewhat premature as is an *a priori* statement which declares stents to be safe at 7.0 T. To respond to the relative lack of data this work performs a careful safety evaluation of RF induced heating of coronary stents. For this purpose electromagnetic field coupling is investigated depending on stent geometry (length, location, orientation), vessel diameter and RF coil used. To meet this goal numerical electromagnetic (EM) and thermal simulations are performed in phantoms and in human voxel models. Simulations were validated by calibrated field probe measurements using an ASTM like phantom together with intracoronary stents common in clinical practice [2].

Methods: E-field coupling was investigated for clinically relevant stent lengths (l < 4 cm), coronary vessel diameters (d < 4 mm) and stent orientations (α = 0-90°) with regard to the E-field vector [3-4]. Stent locations were evaluated up to 12 cm depth which is common for LAD, LCX and RCA stenting [4]. EMF and thermal simulations were conducted with SEMCAD (SPEAG, Zurich, Switzerland) and CST Microwave Studio (CST GmbH, Darmstadt, Germany). For the EMF simulations a stent equivalent (Cu-tube), which provides a reasonable approximation of a coronary stent [5], was used for the sake of simulation time shortening. For the experiments coronary stents (l = 16, 40 and 60 mm, PRO-Kinetic Energy Cobalt Chromium Coronary Stent System, Biotronik, Bülach, Switzerland) were employed (Fig. 1A). A bowtie electric dipole antenna was used for RF transmission in simulations and experiments [6] (Fig. 1B) since this approach generates E-fields such that the Poynting vector is oriented perpendicular to the main axis of the dipole antenna (size: 15 cm) and hence affords defined E-field vectors in relation to the stent. Simulations were performed in materials mimicking myocardial tissue (ε_1 = 58.2, σ_1 = 0.77 S/m). E-field measurements were conducted using an E-field sensor (OEFS-S1B, Seikoh Giken, Japan) in an ASTM like phantom filled with a TWEEN20 water mixture (ε_2 = 59.6, σ_2 = 0.89 S/m) together with a previously proposed calibration method [7]. SAR was evaluated for 1 g mass averages resulting in cubes of V_1 = 1.3 cm³ (Fig. 1C-D). Thermal simulations (mesh = (60x60x60) µm³) were calculated with a CAD model of a stent. SAR assessment was conducted in human voxel models (ITIS Foundation, Zurich, Switzerland) using a TX/RX coil array tailored for CMR at 7 T [8].

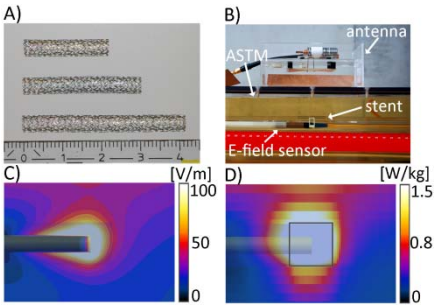

Fig. 1: Picture photograph of A) the investigated stent type and B) the measurement setup. C) E-Field simulations with a stent equivalent showing the antenna effect and D) the resulting SAR_{1g} distribution at its tip.

Results: The results of max SAR_{1g} and max SAR_{10g} (P_{in} = 1 W rms) of the stent configurations are shown in Fig.2. SAR_{10g} results (Fig. 2A-D) average out peak SAR values due to the sheer 10 g volume V_2 = 9.3 cm³ versus the 1 g volume V_1 as indicated in Fig. 1C, D. The more realistic 1 g SAR values were found to be proportional with the power of 2 of the stent length (R^2 = 1) (Fig. 2A). Max SAR_{1g} as a function of stent rotation follows a cosine (R^2 = 1) (Fig. 2B), while a change in stent diameter is not affecting max SAR_{1g} significantly (Fig. 2C). An increase in the distance between the stent and the dipole antenna results in an exponential decay (R^2 = 1) of max SAR_{1g} (Fig. 2D). For a single dipole antenna SAR_{1g} values at the tip of the stent equivalent exceeded surface SAR values for a distance between the dipole and the stent of up to 5.1 cm (Fig. 2D). A linear correlation was found for the induced SAR_{1g} peaks around the stent vs. the baseline SAR distribution w/o stent (Fig. 2D-F). Temperature simulations showed a saturation curve and revealed no local temperature peaks for the stent structure with the exception of the antenna effect at the tip of the stent (Fig. 2G-H). The absolute E-field simulation, measurement and calibration setup is shown in Fig. 3A-C. E-field probe measurements in the ASTM like phantom provided absolute E-fields which were about 12 % inferior to simulations (Fig. 3D) for the baseline (w/o stent), which is due to neglected losses of the dipole antenna. With the stent equivalent, the deviation of the measured E-field at the tip of the stent equivalent was $\Delta|\overrightarrow{E}|$ = -26 % vs. the simulations (Fig. 3E). Notwithstanding this deviation the normalized curves demonstrate a very good qualitative agreement between the simulations and the E-field measurements (Fig. 3F). E-field measurements of a stent (l = 4 cm) showed the antenna effect however with lower peak E-field values vs. Cu-tube (Fig. 3E). SAR evaluations in the human voxel model "Duke" using a stent equivalent placed in close proximity (x = 2 cm) to a 4 channel loop coil revealed a factor of ΔSAR_{max} > 4 when comparing SAR_{1g} vs. SAR_{10g}.

Discussion: Our results show an overall agreement between E-field simulations and E-field measurements. Although our considerations are conservative since thermal heat sinks like blood flow were not included in our model, extra care is required for SAR considerations and RF coil power settings used in patients equipped with coronary stents at 7.0 T. Indeed, our results indicate that SAR_{10g} estimates might severely underestimate local hotspots and temperature changes induced by coronary stents. We anticipate extending our numerical simulations and E-field measurements to TX arrays other than bow tie dipole antennas. These efforts shall include a broad range of RF shim settings to validate and generalize the observations made in this study en route to UHF-MR in patients with intracoronary stents.

Conclusion: Our simulations and measurements provide guidance for the safety assessment of UHF-CMR of patients with intracoronary stents. The approach proposed here can be transferred to a broad range of RF coil designs, stent types and stent configurations including vascular stents, which would be of tremendous help to determine safe RF exposure levels for SAR personalized UHF-MR exams.

References: [1] Niendorf T, et al., JMR, 2012 [2] ASTM F2182-11 [3] Christiansen E, et al., The Lancet, 2013 [4] Bakhai A, et al., Int J. Cardiol.,2004 [5] Santoro D, et al., PLOS ONE, 2012 [6] Winter L, et al., PLOS ONE, 2013 [7] Seifert F, et al., ISMRM Proc., 2011 [8] Dieringer M, et al., JMRI, 2011

Acknowledgements: This work was supported by EMRP grant HLT06. The EMRP is jointly funded by the EMRP participating countries within EURAMET and the European Union.

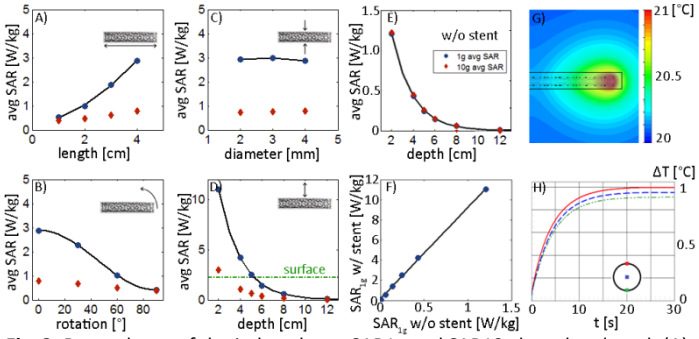

Fig. 2: Dependence of the induced max SAR1g and SAR10g based on length (A), orientation (B), diameter (C) and depth (D) of a stent and w/o a stent (E). Correlation of the 1 g SAR curves w/ and w/o stent equivalent (F). G) Thermal simulations (6 min) of a CAD model of a stent and H) temperature saturation curve (30s) for a stent equivalent.

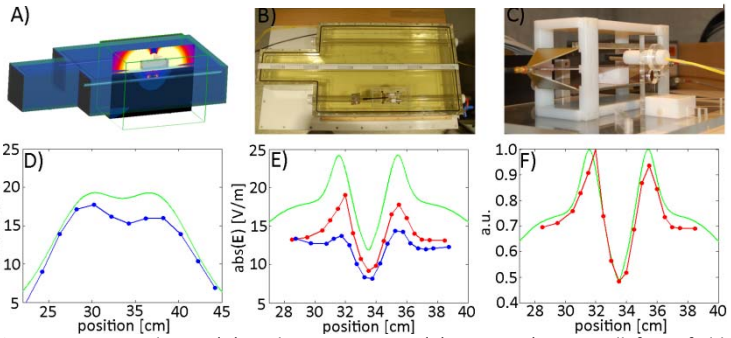

Fig. 3: ASTM simulation (A) and measurement (B) setup. C) TEM cell for E-field sensor calibration. D) Simulations (green) vs. measurements (blue) w/o stent. E) Simulations (green) vs. measurements w/ stent equivalent (red) and stent (blue). F) Normalized comparison of simulations (green) vs. measurements w/ stent (red).